Contract No. NAS8-33107
ADVANCED METHODS FOR PREPARATION AND
CHARACTERIZATION OF INFRARED DETECTOR MATERIALS

Quarterly Progress Report for the
Period 5 June 1979 - 4 September 1979

Submitted to:

National Aeronautics and Space Administration
George C. Marshall Space Flight Center
Marshall Space Flight Center, Alabama 35812
Attention: Code AP29-F

Contractor:

McDonnell Douglas Corporation
McDonnell Douglas Research Laboratories
St. Louis, Missouri 63166

Principal Investigator
S. L. Lehoczky

ADVANCED METHODS FOR PREPARATION AND CHARACTERIZATION OF INFRARED DETECTOR MATERIALS

1. Under NASA Contract No. NAS8-33107, effective 5 December 1978, the McDonnell Douglas Research Laboratories is performing research on $Hg_{1-x}Cd_xTe$ alloys. The objective of this program is to quantitatively establish the characteristics of $Hg_{1-x}Cd_xTe$ grown on Earth as a basis for evaluating the improvements in space-processed material and to develop the theoretical analytical methods required for such evaluation. The research will include the entire range, $0 < x < 1$, of $Hg_{1-x}Cd_xTe$ alloy compositions. Crystals will be prepared by the Bridgman and Te-rich-zone methods for ranges of growth rates and temperature gradients adequate to establish compositional gradients under diffusion-limited and equilibrium growth conditions. The pseudobinary HgTe-CdTe constitutional phase diagram will be determined with precision and used to calculate the segregation coefficient of Cd as a function of x and temperature. Alloy composition gradients for different crystal-growth conditions will be calculated and compared with experimental data to develop a quantitative model of the crystal-growth kinetics for $Hg_{1-x}Cd_xTe$ alloys. Optical absorptance and reflectance spectra from 4.2 to 300 K will be measured and analyzed to determine the temperature and composition dependences of energy-band parameters. Electron and hole mobilities as functions of temperature will be analyzed to establish charge-carrier scattering probabilities. Computer algorithms specific to $Hg_{1-x}Cd_xTe$ alloys will be developed for the calculation of charge-carrier concentration, charge-carrier mobility, Hall coefficient, optical absorptance, and Fermi energy as a function of x, temperature, ionized donor and acceptor concentration, and neutral-defect concentration.

2. Progress for the Period 5 June - 4 September 1979

2.1 High-Temperature Gradient Directional Solidification

During the reporting period, crystal growth runs were performed for $Hg_{1-x}Cd_xTe$ with $x = 0.2$ at growth rates of 0.31 μm/s (L6) and 0.068 μm/s (L7). The ingots were grown from alloys that were precast in fused silica ampoules of 5-mm i.d. and 10-mm o.d. The lengths of the ingots

were about 18 cm. The applied temperature gradients at the growth interface were in the range of 200 to 280°C/cm.

Following the removal from the ampoules, the ingots were cut into slices, and precision density measurements were performed on selected slices from ingot L6 to determine their average compositions. Similar density measurements on slices cut from ingot L7 are in progress. The compositional profile along the growth axis for ingot L6 as deduced from the density measurements is shown in Figure 1.

Density measurements for ingot L4, grown during the last reporting period, have been completed. The compositional profile along the growth axis of the ingot as deduced from the density data is shown in Figure 2.

From ingot L6 several thin slices were prepared for infrared transmission-edge mapping to evaluate the radial compositional variations. The axial positions of the slices along the ingot are shown in Figure 3(a). The infrared measurements were made on each slice at the radial positions shown in Figure 3(b). The diameter of the circles and their positions correspond to the width and relative locations of the incident infrared beam. The thicknesses of the polished and etched slices were between 200 and 210 μm. Typical transmission data for a slice (A26) are shown in Figure 4. The radial variation of the cut-on wavelengths and of the corresponding alloy compositions for a number of the slices are shown in Figure 5. Figure 6 shows the radial variation of the wavelength at 50% transmission. The radial composition profiles suggest concave solid/liquid interfaces for the entire growth length.

The measured longitudinal composition profiles for the ingots L4 and L6 have been compared with the expected theoretical variations for various assumed values for the liquid/liquid diffusion coefficient. These comparisons, along with the results reported for the last quarter, suggest a diffusion coefficient between 5×10^{-5} and 1×10^{-4} cm^2/s. For these initial calculations, we have treated the interface segregation coefficient as being constant during the entire

solidification process. More detailed calculations that include the variations in the segregation coefficients and other aspects associated with the changes in the interface temperature are in progress.

2.2 Pseudobinary HgTe-CdTe Phase Diagram

During the past quarter, a concentrated effort was undertaken to reduce the free-volume in the ampoules used for the differential thermal analysis (DTA) measurements. For this purpose, 5-mm diameter rods, etched in concentrated hydrofluoric acid to achieve close fits, were sealed in the capsules using various sealing configurations. For x-values of 0.3 to 0.9, the procedures repeatedly resulted in rupture of the capsules at the measurement temperatures. The cause of these failures is presently unclear.

Figures 7 and 8 show respectively the DTA results for the surviving $x = 0.1$ and $x = 0.2$ samples. Each figure shows the DTA measurement cycles following 15, 30, and 60 h anneals at the temperatures (T_A) indicated in the figures. The samples are always cooled isothermally to maintain longitudinal alloy homogeneity. The melting point of Sb served as a temperature calibration point. The data do not suggest any significant changes in the DTA curves when the annealing times are increased from 30 to 60 h. Apparently, 30 h annealing near the solidus temperature adequate to eliminate radial inhomogeneities caused by preferential segregation during freezing.

A series of experimental DTA measurements were made to evaluate the behavior of $Hg_{0.8}Cd_{0.2}Te_y$ near the Hg-Te eutectic temperature. For this purpose, 2.844g of Te was placed on top of a cast $Hg_{0.8}Cd_{0.2}Te$ ingot (~0.6 mole) contained in a 5-mm i.d. ampule. The DTA heating curves following the addition of the Te are shown in Figure 9. The differential thermocouple was located at the original $Hg_{0.8}Cd_{0.2}Te/Te$ interface. The maximum temperature of the sample at the termination of each heating run is shown in Table 1. The first DTA curve shows a small exothermic peak which did not occur in any subsequent run. All curves shows a well defined break near the Hg-Te eutectic temperature. The second break in curves 1-4 is interpreted as being due to the melting of

a mixture richer in Te than the eutectic composition. After raising the temperature to 659°C following run 4, only a single endothermic break occurred near the Hg-Te eutectic temperature.

2.3 Calculation of the Partial Pressures of Hg, Cd, and Te Vapor in Equilibrium with $Hg_{1-x}Cd_xTe$ Melts

The phase equilibria calculations, based on the regular associated solution (R.A.S.) theory summarized in Appendix A, have continued. An updated set of R.A.S. parameters were obtained by least-squares fitting to available phase diagram data, both binary and pseudobinary. The results of the calculations are summarized in Table 2. Using the set of R.A.S. parameters listed in Table 2, the activities of Hg, Cd, and Te_2 and their partial pressures over the pseudobinary melt were calculated by the method described in Appendix B. Table 3 lists the latest results, as well as some experimental partial pressures based on measurements by Steininger[1].

The calculated mercury partial pressures are in reasonable agreement with Steininger's experimental results[1]. However, the values of the R.A.S. parameters, and consequently the calculated partial pressures, are extremely sensitive to the detailed compositional dependences of the pseudobinary liquidus and solidus temperatures. We feel, therefore, that further improvements in the accuracy of the liquidus and solidus temperature values for the higher x region will result in significant improvement in the consistency of the various calculated and measured results.

S. L. Lehoczky
Principal Investigator

Appendix A: Regular Associated Solution (R.A.S.) Theory

For our phase equilibria calculations, we assume that the solutions $Hg_{1-x}Te_x$ and $Cd_{1-x}Te_x$ are either regular[2,3,4] or regular associated solutions[5,6,7]. The term "regular solution" was introduced by Hildebrand[2] to describe mixtures whose behavior was found experimentally to have certain regularities. The definition was essentially an empirical one. Guggenheim[3] used the term to describe any mixture of molecules satisfying the conditions for forming an ideal mixture (ideal in the sense of an ideal gas) except that the interchange energy (or interaction parameter as it is sometimes called is not zero. The interaction parameter is related to the nearest neighbor pairwise interaction energies between atoms.

Subsequently, Jordan[5] discussed association in the liquid phase of type A atoms with type B atoms, i.e., the formation of AB species. If the lifetime of the species is long in comparison to the period of vibrations of the atoms, then one can speak of association in the liquid. Jordan did a thermodynamic treatment of associated solutions without considering in detail the type of the bonds involved. This treatment involved an association parameter β, where for a completely associated solution, $\beta = 0$, while for a completely dissociated or regular solution, $\beta = 1$. Jordan labeled his treatment regular associated solution (R.A.S.) theory.

In the context of R.A.S, the liquidus and solidus ternary equations for an A-B-C system are given by[7]:

$$(1-y)\exp\left[\frac{W}{RT}\ y^2\right] = \frac{x_{AC}}{x_{AC}^*}\exp\left[\frac{\Delta H_1+\omega x_2(1-2x_1)+(\alpha_1 x_1+\alpha_2 x_2-0.5\alpha_1)(1-2x_3)}{RT}-\frac{\Delta S_1}{R}\right], \tag{A1}$$

and

$$y\exp\left[\frac{W}{RT}(1-y)^2\right] = \frac{x_{BC}}{x_{BC}^*}\exp\left[\frac{\Delta H_2+\omega x_1(1-2x_2)+(\alpha_1 x_1+\alpha_2 x_2-0.5\alpha_2)(1-2x_3)}{RT}-\frac{\Delta S_2}{R}\right], \tag{A2}$$

where y is the mole fraction of the complex BC in the solid phase, x_1, x_2, and x_3 are the atom fractions of the three components A, B, and C, respectively, x_{AC} and x_{BC} are the mole fractions of the corresponding liquid phase species, and the other parameters are defined in the list of symbols of Appendix C.

For the pseudobinary case, $x_3 = 0.5 = x_1 + x_2$, so that Eqs. (A1) and (A2) become

$$(1-y)\exp\left[\frac{W}{RT}y^2\right] = \frac{x_{AC}}{x_{BC}^*}\exp\left[\frac{\Delta H_1 + \omega x_2(1-2x_1)}{RT} - \frac{\Delta S_1}{R}\right], \tag{A3}$$

and

$$y\exp\left[\frac{W}{RT}(1-y)^2\right] = \frac{x_{BC}}{x_{BC}^*}\exp\left[\frac{\Delta H_2 + \omega x_1(1-2x_2)}{RT} - \frac{\Delta S_2}{R}\right]. \tag{A4}$$

The values for x_{AC}, x_{AC}^*, x_{BC}, and x_{BC}^* are obtained as follows.

The mole fractions of the species in the liquid phase are[6]

$$x_A = x_1(1 + x_{AC} + x_{BC}) - x_{AC}, \tag{A5}$$

$$x_B = x_2(1 + x_{AC} + x_{BC}) - x_{BC}, \tag{A6}$$

and

$$x_C = x_3(1 + x_{AC} + x_{BC}) - x_{AC} - x_{BC}. \tag{A7}$$

The equilibrium constants K_1 (for the binary system AC) and K_2 (for the binary system BC) are related to the R.A.S. parameters α_1, β_1 and α_2, β_2, respectively, by the equations[7]

$$K_1\exp\left(\frac{-\alpha_1}{2RT}\right) = \frac{\beta_1^2}{1-\beta_1^2} \equiv \kappa_1, \tag{A8}$$

$$K_2\exp\left(\frac{-\alpha_2}{2RT}\right) = \frac{\beta_2^2}{1-\beta_2^2} \equiv \kappa_2. \tag{A9}$$

Using these equations and the relations given by Eqs. (A5)-(A7), we obtain explicit expressions for the mole fractions x_A, x_B, x_C, x_{AC} and x_{BC} in terms of x_1, x_2, x_3 and the binary parameters K_1 and K_2. This involves solving the following cubic equation in σ ($\equiv x_{AC} + x_{BC}$):

$$\frac{x_1}{\kappa_1 + 0.5\ (1-\sigma)} + \frac{x_2}{\kappa_2 + 0.5\ (1-\sigma)} + \frac{\sigma}{0.5\ (1-\sigma^2)} . \tag{A10}$$

The mole fractions x_C, x_{AC}, and x_{BC} are then obtained from the equations

$$x_C = 0.5\ (1+\sigma) - \sigma, \tag{A11}$$

$$x_{AC} = \frac{x_1 x_C\ (1+\sigma)}{\kappa_1 + x_c} , \tag{A12}$$

and

$$x_{BC} = \frac{x_2 x_c\ (1+\sigma)}{\kappa_2 + x_C} . \tag{A13}$$

The other mole fractions x_A and x_B are then obtained from Eqs. (A5)-(A7).

The values of the stoichiometric compositions x_{AC}^* and x_{BC}^* are obtained from the binary R.A.S. parameters:

$$x_{AC}^* = 1 - 2\ [\ \kappa_1(1+\kappa_1) - \kappa_1] \tag{A14}$$

$$x_{BC}^* = 1 - 2\ [\ \kappa_2\ (1+\kappa_2) - \kappa_2]. \tag{A15}$$

Appendix C:: List of Symbols

T	=	temperature
ΔS_1, ΔS_2	=	entropies of fusion of the binary systems AC and BC
ΔH_1, ΔH_2	=	heats of fusion of the binary systems AC and BC
R	=	the universal gas constant
α_1	=	the interaction parameter for the liquid binary system AC
α_2	=	the interaction parameter for the liquid binary system BC
ω	=	the interaction parameter between species A and B
W	=	the interaction parameter between species AC and BC in the solid
$*$	=	This superscript is used to denote standard states of the liquid phase (stoichiometric compositions in the binary systems AC and BC).

Appendix B: Component Partial Pressure Over the Pseudobinary Melt

For a ternary regular associated solution of species A, B, and C, the activities a_A, a_B, and a_C are given by the expressions:

$$a_A = x_A\gamma_A = [x_1(1 + x_{AC} + x_{BC}) - x_{AC}]\gamma_A, \tag{B1}$$

$$a_B = x_B\gamma_B = [x_2\ (1 + x_{AC} + x_{BC}) - x_{BC}]\gamma_B, \tag{B2}$$

and

$$a_C = x_C\gamma_C = [x_3\ (1 + x_{AC} + x_{BC}) - x_{AC} - x_{BC}]\gamma_C, \tag{B3}$$

where γ_A, γ_B, and γ_C are the activity coefficients, which are, for the pseudobinary case:

$$\gamma_A = \exp\left[\frac{\omega x_2^{\,2} + 0.25\ \alpha_1 + (\omega + \alpha_1 - \alpha_2)\ (0.5\ x_2)}{RT}\right], \tag{B4}$$

$$\gamma_B = \exp\left[\frac{\omega x_1^{\,2} + 0.25\ \alpha_2 + (\omega - \alpha_1 + \alpha_2)\ (0.5\ x_1)}{RT}\right], \tag{B5}$$

and

$$\gamma_C = \exp\left[\frac{\alpha_1 x_1^{\,2} + \alpha_2 x_2^{\,2} + (\alpha_1 + \alpha_2 - \omega)x_1x_2}{RT}\right], \tag{B6}$$

and the other parameters are defined in Appendix A. For the case of $Hg_{1-x}Cd_xTe$, the partial pressures of the components over the pseudobinary melt, P_{Hg}, P_{Cd}, and P_{Te_2}, are given by

$$P_{Hg} = a_{Hg}P^0_{Hg} \tag{B7}$$

$$P_{Cd} = a_{Cd}P^0_{Cd} \tag{B8}$$

$$P_{Te_2} = a^2_{Te}\ P^0_{Te_2}. \tag{B9}$$

References

(1) J. Steininger, J. Electronic Mat. 5, 299 (1976).

(2) J. H. Hildebrand and R. L. Scott, The Solubility of Non-Electrolytes, 3rd Ed., Reinhold Publishing Corp., New York (1950).

(3) E. A. Guggenheim, Proc. Roy. Soc. A148, 304 (1935).

(4) L. J. Vieland, Acta Met. 11, 137 (1963).

(5) A. S. Jordan, Met. Trans. 1, 239 (1970).

(6) A. Langier, Revue de Physique Appliquee 8, 259 (1973).

(7) S. Szapiro, J. Electronic Mat. 5, 223 (1976).

(8) J. Steininger, J. Appl. Phys. 41, 2713 (1970).

Table 1. Maximum temperature at the end of each heating run in Fig. 9.

Run	Maximum temperature (°C)
1	468
2	498
3	496
4	659
5	659

Table 2 R.A.S. and thermodynamic data for the Hg-Cd-Te system. The subscript 1 refers to HgTe while the subscript 2 refers to CdTe.

R.A.S. parameters*	Thermodynamic data
K_1 = 0.1543	ΔS_1 = 9.2 e.u.[8] = 38.5 J/mol K[(8)]
α_1 = 3481 = 14565 J/mol	ΔS_2 = 8.8 e.u.[8] = 36.8 J/mol K[(8)]
K_2 = 0.05737	ΔH_1 = 8675.6 cal/mol[8] = 36299 J/mol[(8)]
α_2 = 9661 = 40422 J/mol	ΔH_2 = 12012 cal/mol[8] = 50258 J/mol[(8)]
ω = 7219 = 30204 J/mol	T_1 = 943 K
W = 2761 = 11552 J/mol	T_2 = 1365 K

*The values of K_1, α_1, K_2, and α_2 were obtained from the metal rich sides of the binary phase diagrams for $Hg_{1-x}Te_x$ and $Cd_{1-x}Te_x$, as part of an IRAD investigation.

Table 3 Calculated values of component partial pressures in the $Hg_{1-x}Cd_xTe$ system using R.A.S. theory

T (K)	x	a_{Hg}	a_{Cd}	a_{Te}	P_{Hg}	P_{Cd}	P_{Te_2}	P_{Hg}*	P_{Cd}	P_{Te_2}
					atm.					
1098.2	0.276	0.22	0.16	0.25	117	1.91	0.20	26(40)	0.30	0.013
1123.2	0.326	0.23	0.15	0.25	135	2.44	0.26	31(47)	0.36	0.017
1148.2	0.380	0.24	0.14	0.25	155	3.09	0.34	37(53)	0.44	0.022
1173.2	0.440	0.25	0.14	0.26	177	3.88	0.44	44(61)	0.53	0.029
1198.2	0.500	0.25	0.13	0.26	201	4.82	0.56	50(69)	0.63	0.037
1223.2	0.560	0.26	0.12	0.26	227	5.93	0.70	58(78)	0.74	0.047
1248.2	0.620	0.26	0.12	0.26	255	7.25	0.88	66	0.84	0.060
1273.2	0.690	0.26	0.10	0.26	286	8.78	1.09	76	0.91	0.077
1298.2	0.760	0.27	0.09	0.27	318	10.6	1.34	86	0.94	0.098
1323.2	0.826	0.28	0.07	0.28	353	12.6	1.64	97	0.90	0.124

*For the activity coefficient of Hg, Steininger[1] obtained the value of 0.345 ± 0.020 from experimental data. The partial pressures in parentheses were calculated using this value.

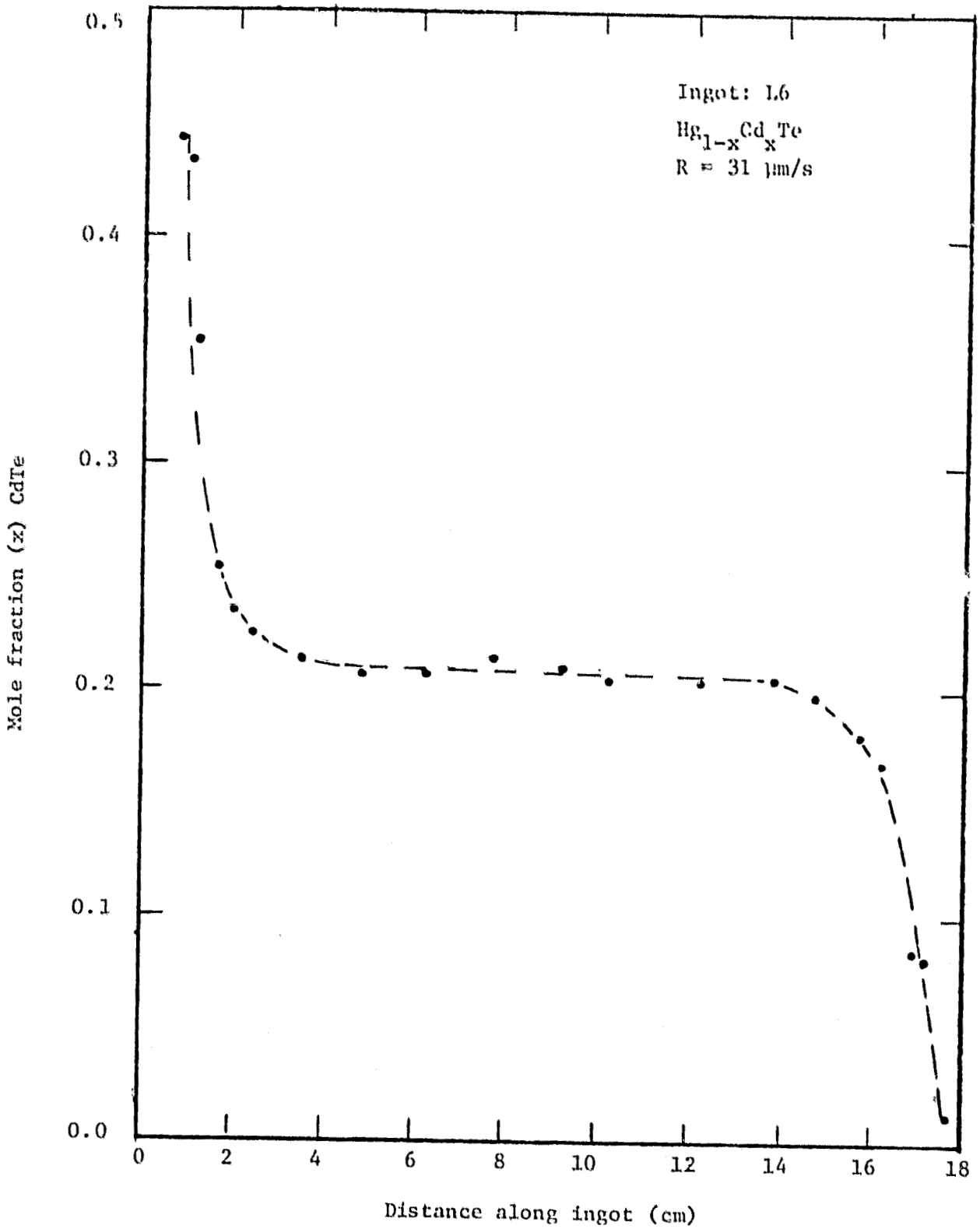

Figure 1. Experimental variation of the axial composition of ingot L6 for a growth rate of R = 0.31 μm/s.

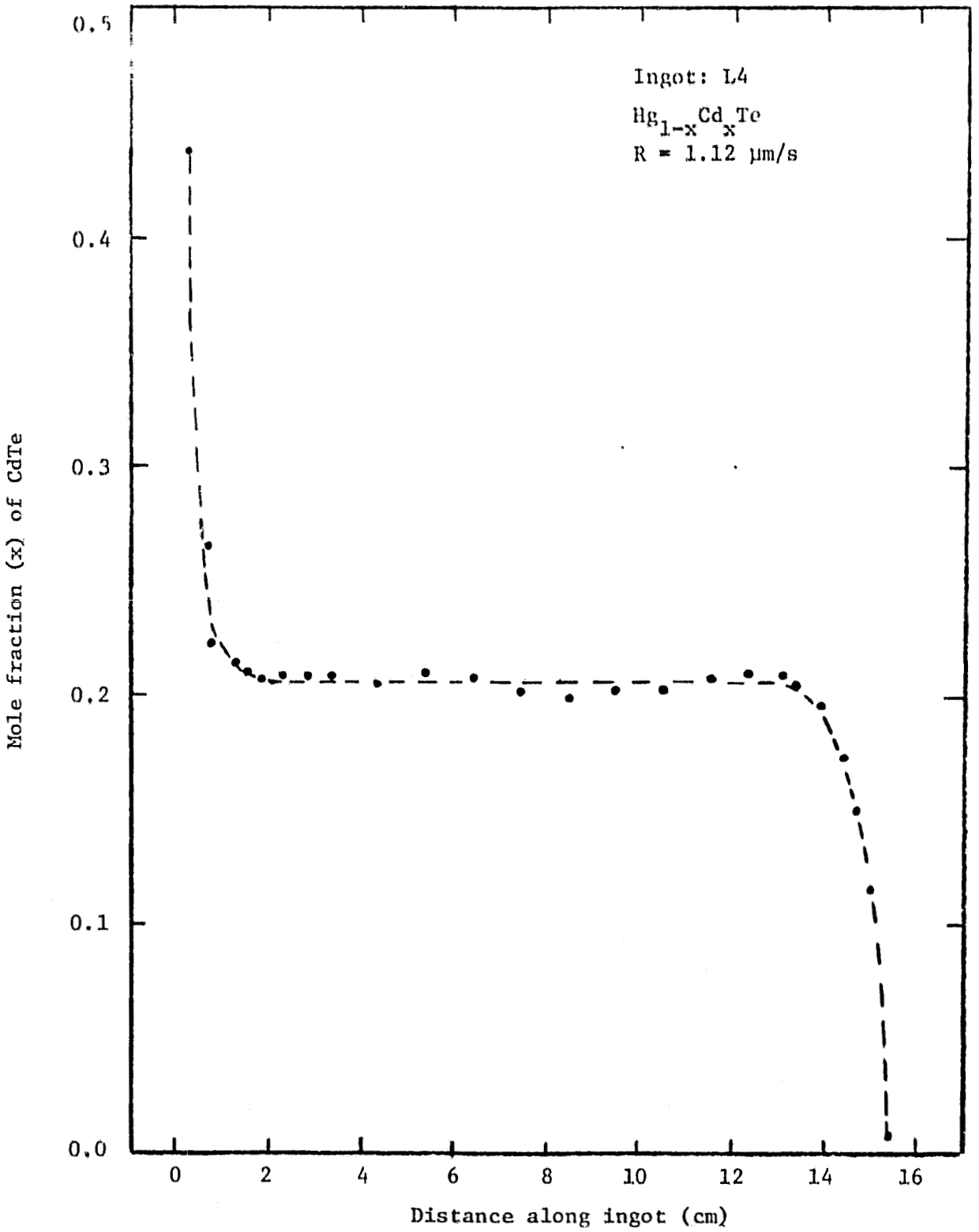

Figure 2. Experimental variation of the axial composition of ingot L4 for a growth rate of R = 1.12 μm/s.

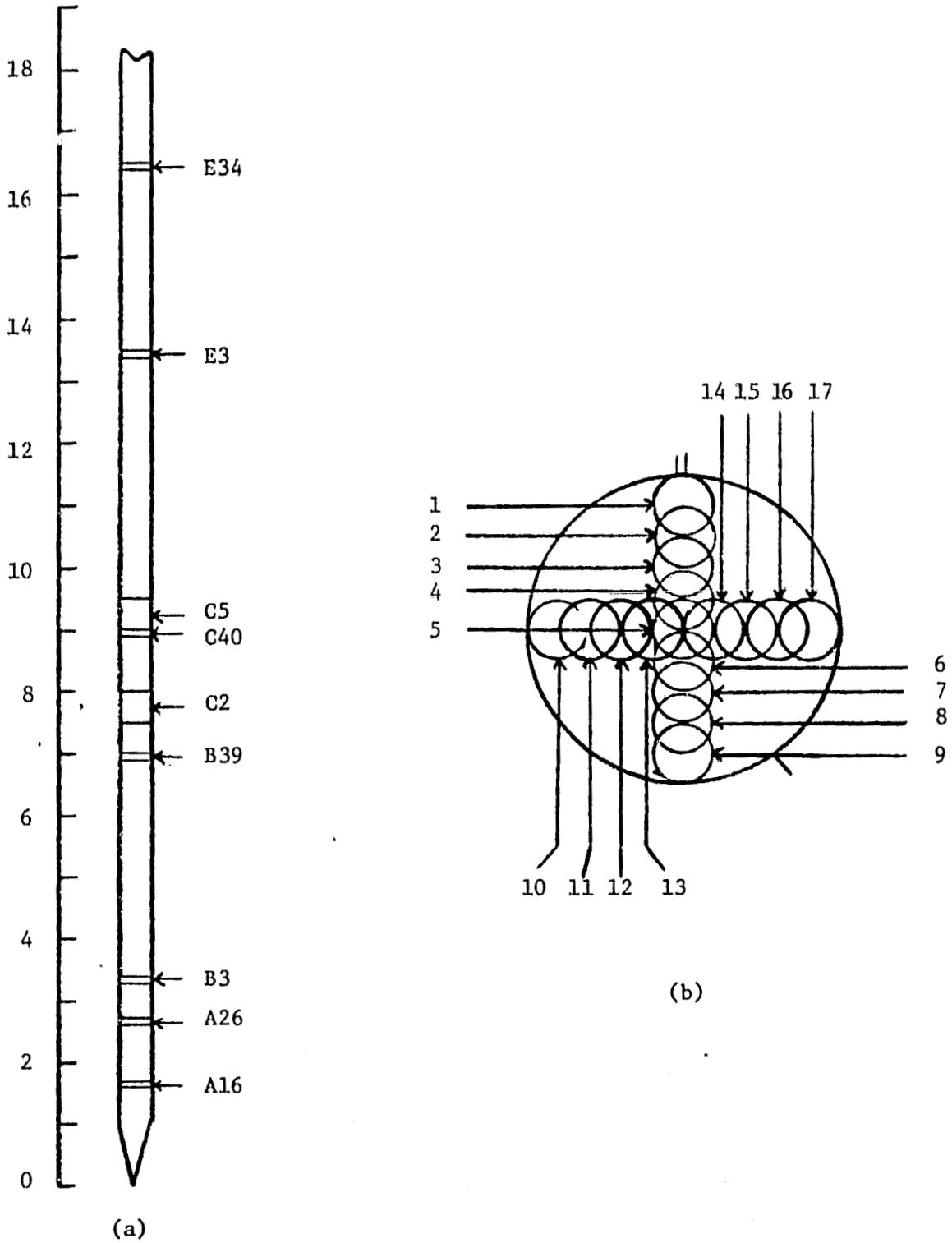

Figure 3. Location of wafers along the growth axis of ingot L6 (a) and the IR measurement positions for a wafer (b).

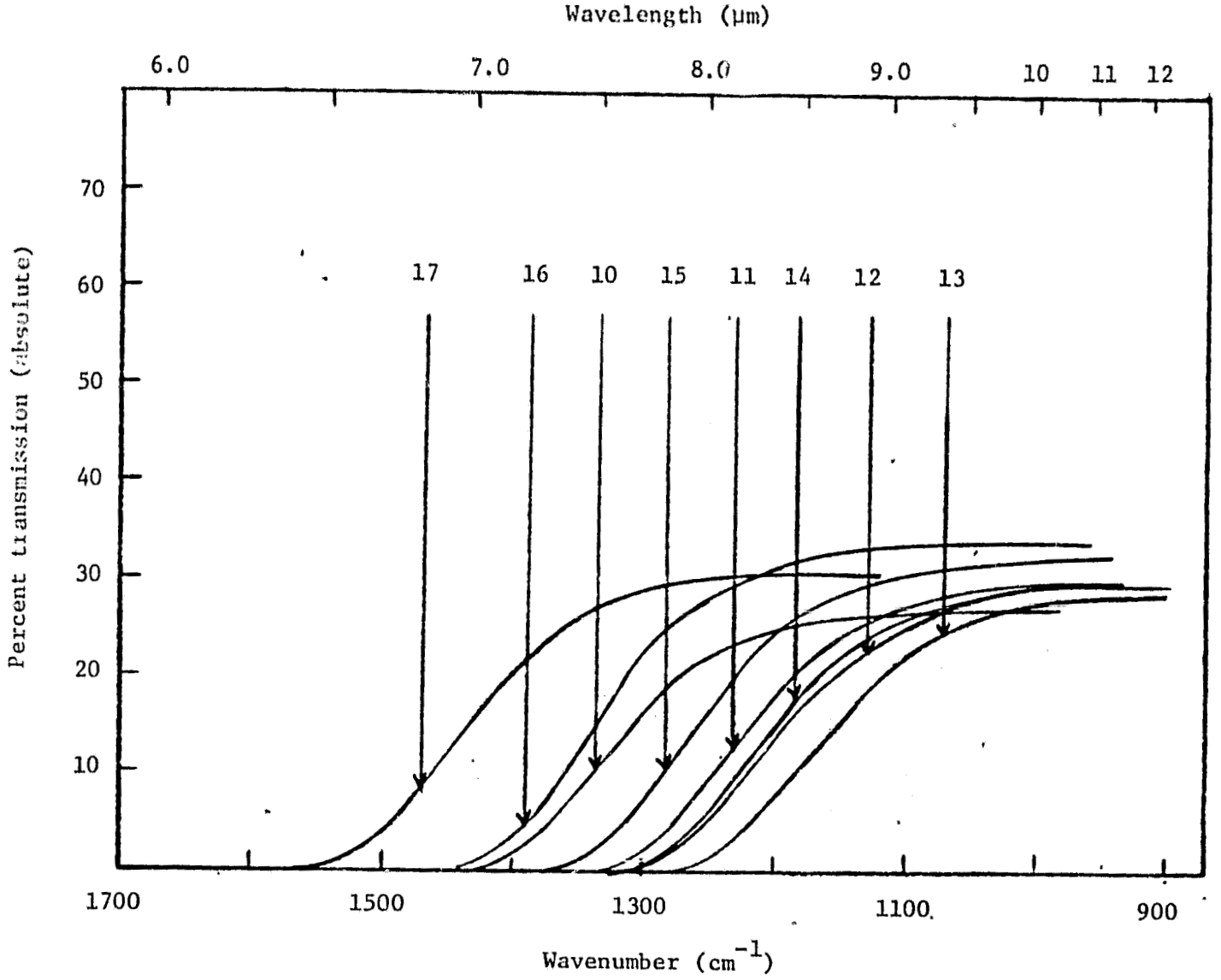

Figure 4. Typical transmission spectra for a wafer (A26) from ingot L6. The thickness of the polished slice was 200 μm. The numbers in the figure indicate the measurement positions as defined in figure 3b.

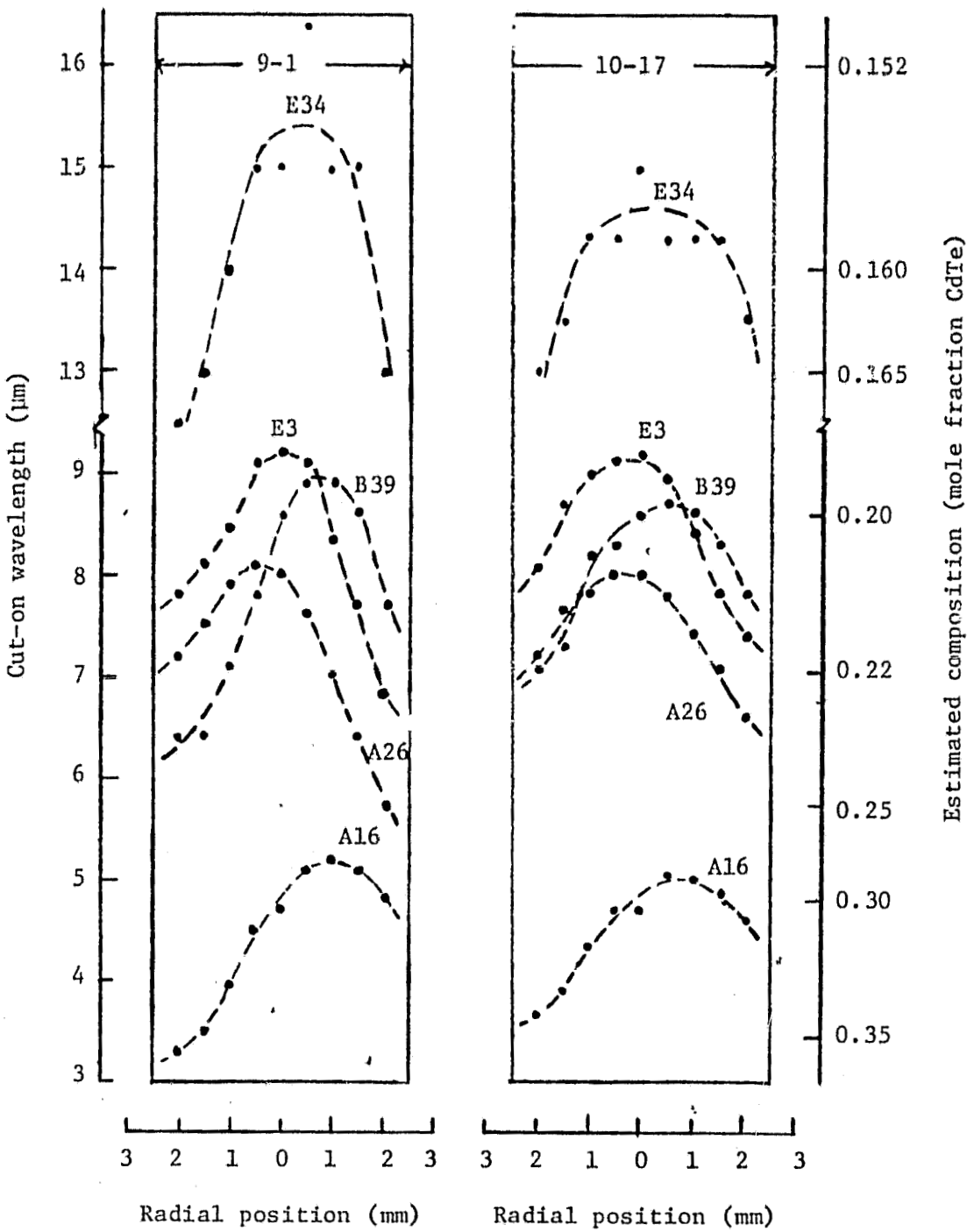

Figure 5. Variation of cut-on wavelength and composition across slices from ingot L6. The location of the slices are defined in figure 3a.

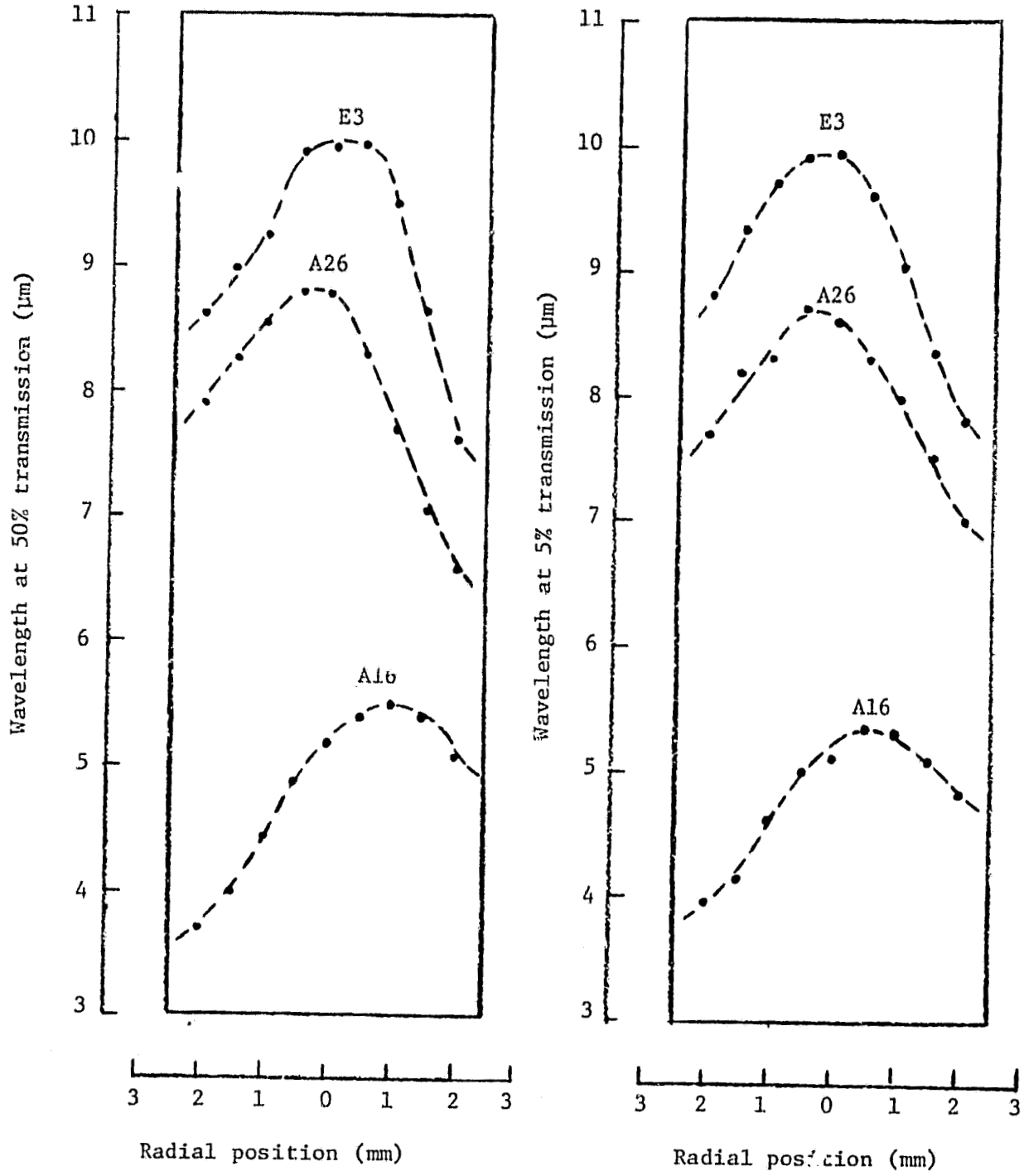

Figure 6. Radial variation of wavelength at 50% relative transmission across slices from ingot L6. The location of the slices are defined in figure 3a.

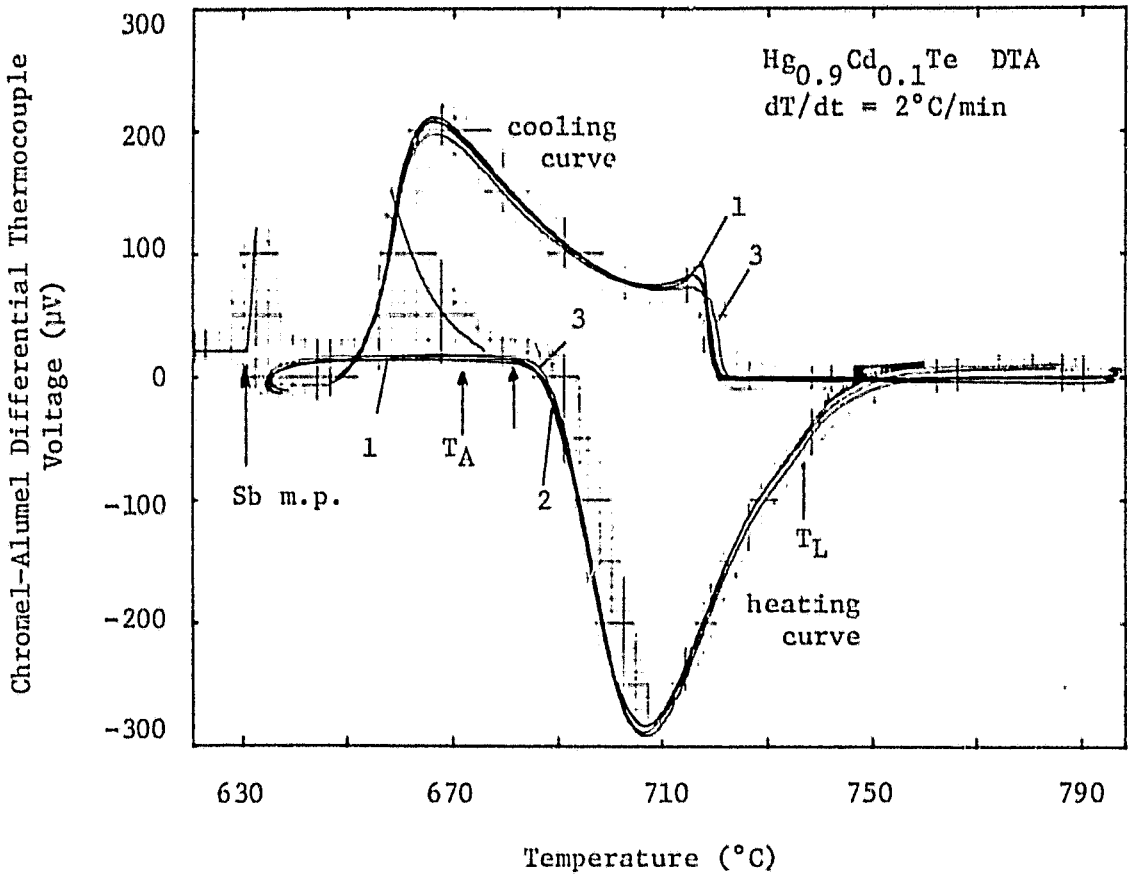

Figure 7. Differential thermal analysis data for $Hg_{0.900}Cd_{0.100}Te$. The Sb melting point shown in the figure is used as a calibration point. T_A is the annealing temperature and T_L the liquidus. Curves 1, 2, and 3 followed 15 h, 30 h, and 60 h, annealing times, respectively.

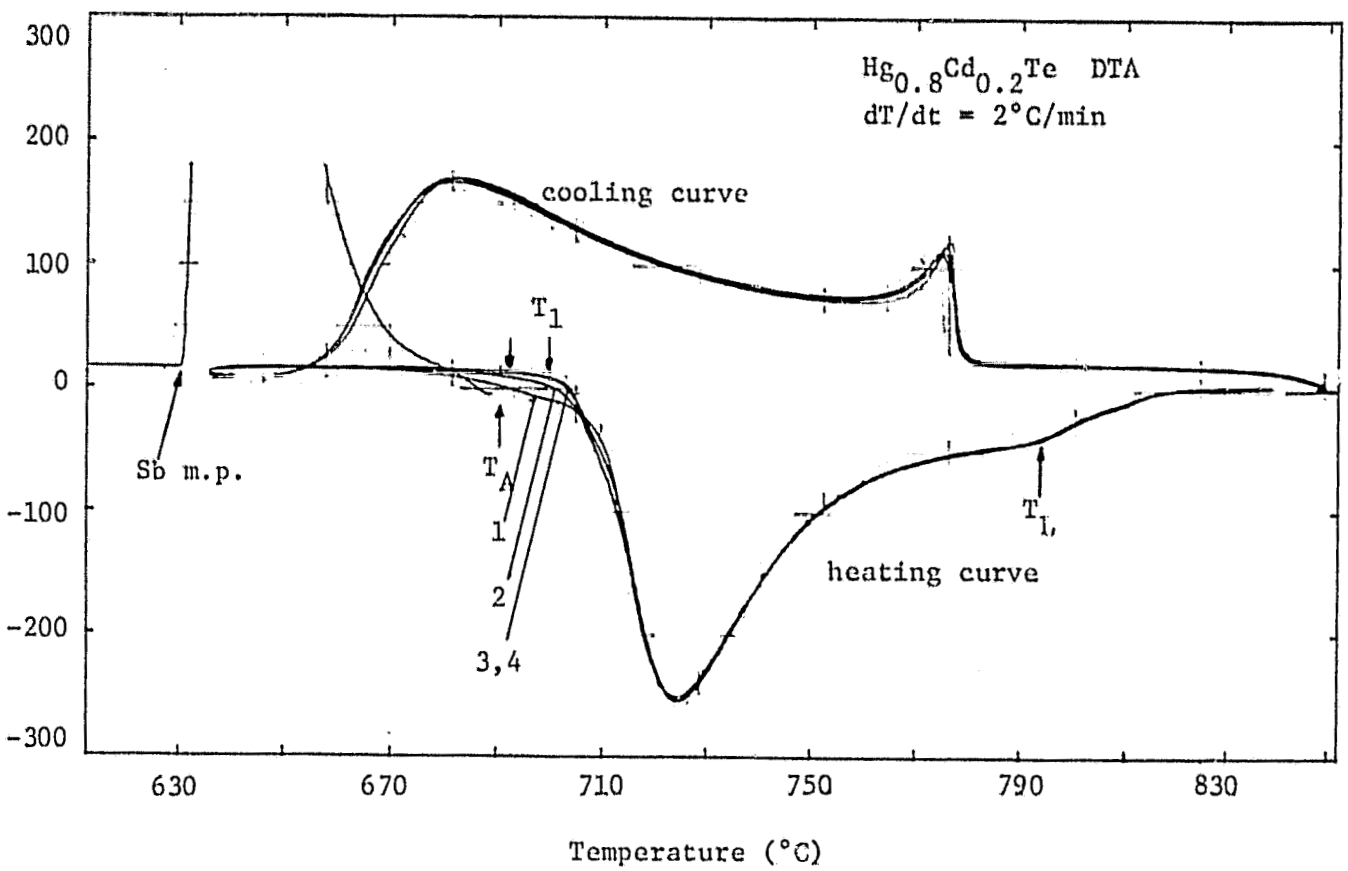

Figure 8. Differential thermal analysis data for $Hg_{0.800}Cd_{0.200}Te$. The Sb melting point shown in the figure is used as a calibration point. T_A is the annealing temperature, and T_L the liquidus. Curve 1 followed 42 h at T_1. Curves 2, 3, and 4 followed 15 h, 30 h, and 60 h annealing times at T_A.

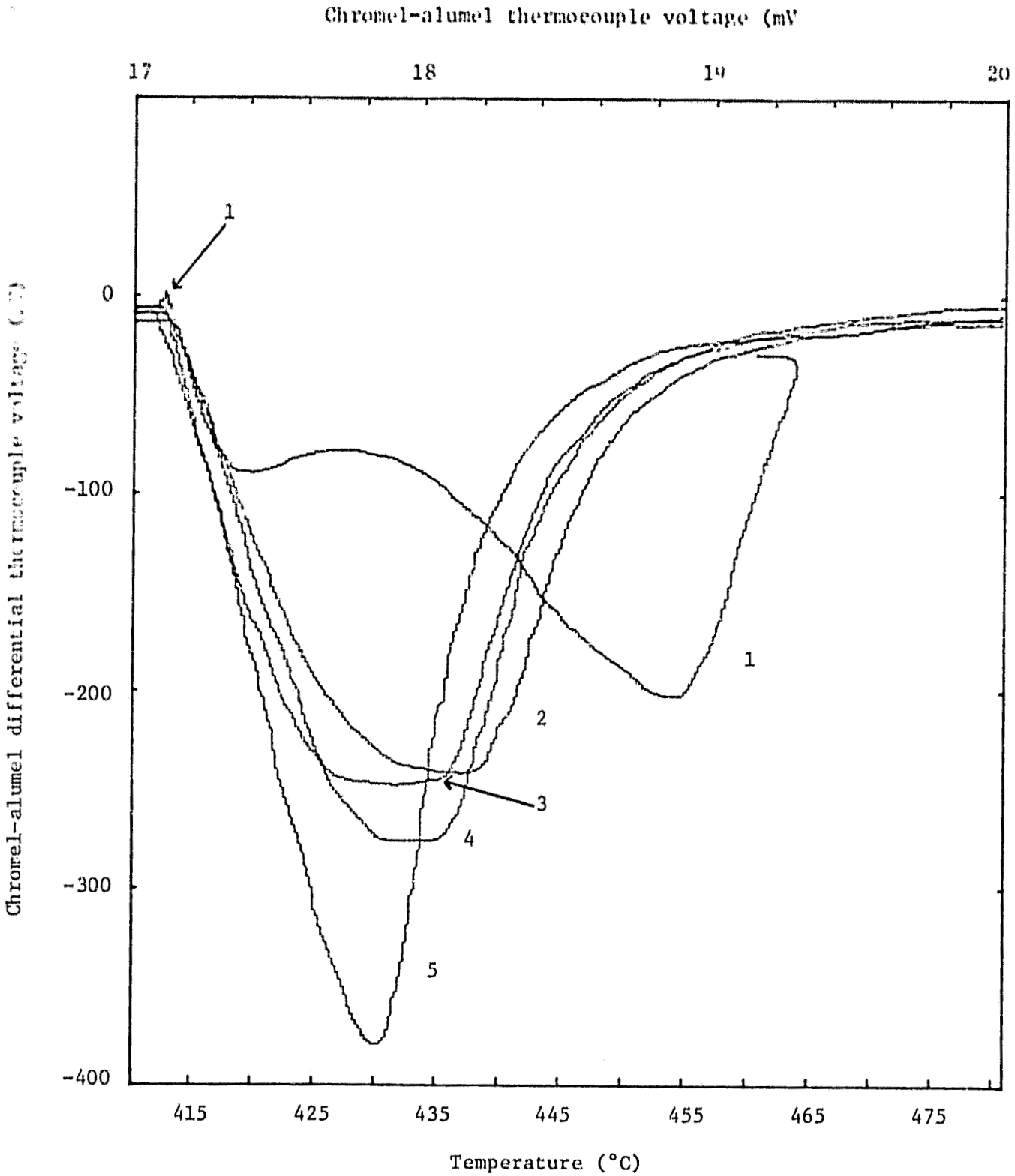

Figure 9. Differential thermal analysis data for $Hg_{0.8}Cd_{0.2}Te$ with excess Te added.